Can. J. Remote Sensing, Vol. 34, Suppl. 2, pp. S1–S18, 2008

Production of vegetation spatial-structure maps by per-object analysis of juniper encroachment in multitemporal aerial photographs

Alistair M.S. Smith, Eva K. Strand, Caiti M. Steele, David B. Hann, Steven R. Garrity, Michael J. Falkowski, and Jeffrey S. Evans

Abstract. The remote sensing of vegetation, which has predominantly applied methods that analyze each image pixel as independent observations, has recently seen the development of several methods that identify groups of pixels that share similar spectral or structural properties as objects. The outputs of "per-object" rather than "per-pixel" methods represent characteristics of vegetation objects, such as location, size, and volume, in a spatially explicit manner. Before decisions can be influenced by data products derived from per-object remote sensing methods, it is first necessary to adopt methodologies that can quantify the spatial and temporal trends in vegetation structure in a quantitative manner. In this study, we present one such methodological framework where (*i*) marked point patterns of vegetation structure are produced from two per-object methods, (*ii*) new spatial–structural data layers are developed via moving-window statistics applied to the point patterns, (*iii*) the layers are differenced to highlight spatial–structural change over a 60 year period, and (*iv*) the resulting difference layers are evaluated within an ecological context to describe landscape-scale changes in vegetation structure. Results show that this framework potentially provides information on the population, growth, size association (nonspatial distribution of large and small objects), and dispersion. We present an objective methodological comparison of two common per-object approaches, namely image segmentation and classification using Definiens software and two-dimensional wavelet transformations.

Résumé. La télédétection de la végétation, qui consistait principalement en l'application de méthodes analysant chacun des pixels de l'image comme des observations indépendantes, a vu récemment le développement de plusieurs méthodes qui identifient des groupes de pixels partageant des propriétés spectrales ou structurelles comme des objets. Les produits des méthodes « par-objet », plutôt que « par-pixel » représentent les caractéristiques des objets de type végétation telles que la localisation, la dimension, le volume, etc., d'une façon spatialement explicite. Avant que des décisions ne puissent être influencées par des produits de données dérivés des méthodes de télédétection par-objet, il est nécessaire au départ d'adopter des méthodologies permettant de quantifier les tendances spatiales et temporelles dans la structure de la végétation de façon quantitative. Dans cette étude, nous présentons l'ébauche d'une telle méthodologie où (*i*) des patrons de points caractéristiques de la structure de la végétation sont produits à l'aide de deux méthodes par-objet; (*ii*) des nouvelles couches de données spatiales-structurelles sont développées par le biais de statistiques basées sur les fenêtres mobiles appliquées aux patrons de points; (*iii*) les couches sont différenciées pour mettre en relief le changement spatial-structurel au cours d'une période de 60 ans; et (*iv*) les couches de différences résultantes sont évaluées dans un contexte écologique pour décrire les changements dans la structure de la végétation à l'échelle du paysage. Les résultats montrent que ce cadre procure potentiellement une information sur la population, la croissance, l'association par taille (répartition non spatiale de gros et de petits objets) et la dispersion. Nous présentons une comparaison méthodologique objective de deux approches par-objet fréquemment utilisées : la segmentation et la classification d'images à l'aide du logiciel Definiens et des transformations en ondelettes 2D.
[Traduit par la Rédaction]

Received 23 February 2008. Accepted 25 July 2008. Published on the *Canadian Journal of Remote Sensing* Web site at http://pubs.nrc-cnrc.gc.ca/cjrs on XX XXXX 2008.

A.M.S. Smith,[1,2] E.K. Strand,[2] S.R. Garrity,[2] and M.J. Falkowski. College of Natural Resources, University of Idaho, Moscow, ID 83844, USA.

C.M. Steele. Jornada Experimental Range, US Department of Agriculture Agricultural Research Service, New Mexico State University, Las Cruces, NM 88003, USA.

D.B. Hann. Department of Mechanical Engineering, University of Nottingham, Nottingham NG7 2RD, UK.

J.S. Evans. Rocky Mountain Research Station, US Department of Agriculture Forest Service, Moscow, ID 83844, USA.

[1]Corresponding author (e-mail: alistair@uidaho.edu).
[2]These authors contributed equally to this paper.

Vol. 34, Suppl. 2, 2008

Introduction

Terrestrial remote sensing has largely been limited to analyzing the *z* dimension of individual pixels (e.g., spectral reflectance, spectral index value, elevation) without explicitly considering the spatial arrangement of contiguous pixels that share similar *z* dimensions (Burnett and Blaschke, 2003; Groome et al., 2006). Per-pixel classifications of passive data are often achieved by assigning classes based on defining thresholds (manual or statistical) within a given cover type training dataset. An exception is "texture wavebands" (Atkinson and Lewis, 2000; Berberoglu et al., 2007), which have been used to enhance *z*-based classifications (Berberoglu et al., 2000; Lark, 1996). Another textural analysis exception is co-occurrence matrices, where variances of spatially adjacent (but often offset) operators are used in image segmentation (Haralick et al., 1974; Carlson and Ebel, 1995; Paplinksi and Boyce, 1997; Hann et al., 2003; Coburn and Roberts, 2004). To distinguish between texture analyses and true per-object methods, texture analyses often provide information about the variance within pixel assemblages, rather than separate information on each individual image object (Hudak and Wessman, 1998; Smith et al., 2002; Asner et al., 2003; Wang et al., 2004a; Wulder et al., 2004).

Tree crown extraction exemplifies the limitations of per-pixel classification approaches. Per-pixel classification of high spatial resolution imagery (e.g., <5 m) may result in contiguous pixels within a single crown classified differently, as tree or no tree, producing classifications with a speckled appearance. The limitations of the per-pixel approach coupled with the ever-increasing availability of very high spatial resolution (<2 m) remote sensing data from aerial photography and light detection and ranging (lidar) have led to the widespread interest in per-object remote sensing methods (Lucieer et al., 2005; Zhan et al., 2005), which identify spatially distinct assemblages of pixels that share similar *z*-dimension properties as discrete objects (Hall et al., 2003; Lucieer et al., 2005; Groome et al., 2006). Once pixels within an individual object have been identified and grouped, the pixel values within and between objects can then be analyzed to characterize object-specific properties. The interaction between pixels, objects, and cover maps is depicted in **Figure 1**.

The output of any per-object classification can be summarized by marked point patterns (Diggle, 2003; Strand et al., 2006b), where each point represents the location of an object and is attributed with a continuous value representing the size or magnitude of the object (e.g., tree crown width, maximum tree height). Although adopted less often, per-pixel classifications can also produce a marked point pattern by converting classified pixels to polygons, followed by assigning a single point to each polygon. Before land management can incorporate data products derived from these remotely sensed per-object or converted per-pixel methods in decision making, it is necessary to develop (*i*) per-object interpretation

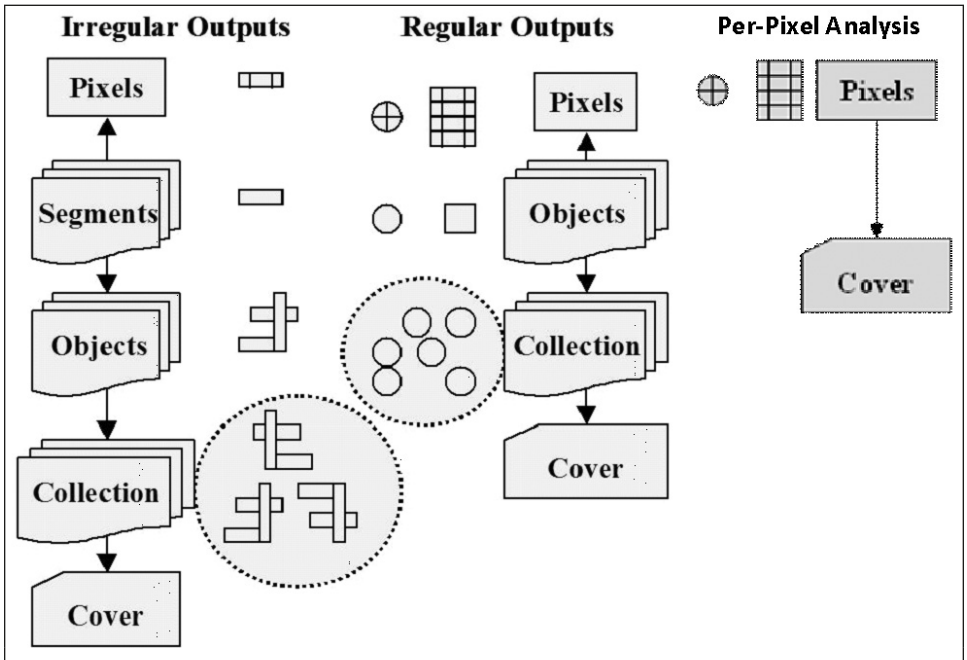

Figure 1. Schematic of per-object and per-pixel remote sensing and proposed per-object terminology. In per-object remote sensing, groups of pixels can be identified and aggregated to produce segments (one-dimensional strips) and objects (two or three dimensions). A collection can be defined as a group of similar or comparable objects within a reasonably defined extent, e.g., canopy gaps within a stand or junipers within a watershed. Aggregation of all collections of a given object type within an image would produce a cover map. In per-pixel analysis, each pixel is analyzed in an independent manner, and such an output could directly be a cover map.

methodologies, which must describe the structure of the objects in a spatially and temporally explicit manner and produce new data layers for future per-object classifications; and (*ii*) per-object accuracy assessment methodologies, which must robustly evaluate the ability of per-object methods to not only detect the presence–absence but also accurately characterize the structural properties (location; horizontal, vertical, and volumetric shapes; etc.) of the detected image objects.

Per-object accuracy assessment should consider approaches that properly penalize methods that can identify the location but not the correct size–shape of the object. For example, Zhan et al. (2005) highlighted the need to examine not only the "classification quality" or omission and co-omission errors but also the "geometric quality" as defined by the shape, spatial location, spatial extent, and size of the image objects. Contemporary studies (e.g., Falkowski et al., 2008; Garrity et al., 2008) are considering the application of statistical equivalence tests (Robinson and Froese, 2004; Robinson et al., 2005), which can evaluate whether a set of remotely sensed object metrics (e.g., maximum tree heights) are statistically equivalent and unbiased when assessed against the comparable set of field-measured object metrics. These tests can be used alongside traditional metrics that assess the quantity of omission and co-omission errors, such as through the application of confusion matrices (Hall et al., 2003; Lucieer et al., 2005; Gao et al., 2006). However, extra care is advised when evaluating per-object analyses with a confusion matrix because per-object methods may detect additional objects not included within the field survey but that may actually be correctly classified (e.g., trees smaller than a field-designated minimum diameter at breast height). Conversely, the per-object methods may detect erroneous additional objects that were not recorded in the field inventory (e.g., large boulders, structures). To properly apply confusion matrices, a 100% inventory of all "potential" objects is needed, which may not be feasible.

In this study, per-object interpretation methodologies were evaluated by demonstrating how the outputs of any per-object remote sensing method can be applied within a temporal data integration framework to produce a new set of spatially explicit data layers. Given the widespread application of Definiens software and the increasing use of two-dimensional (2D) wavelet transformations (WTs) to produce per-object information, we describe in full how per-object data are produced using each method. We discuss the advantages, disadvantages, and accuracy that each approach presents when applied to identify juniper encroachment in multitemporal aerial photography.

Background: per-object remote sensing approaches

Several per-object approaches have been developed and applied to remote sensing of vegetation (Palenichke and Zaremba, 2007), including (*i*) individual tree detection methods using lidar data (e.g., Leckie et al., 2003a; Popescu et al., 2003; Popescu and Wynne, 2004; Falkowski et al., 2006); (*ii*) the application of hand-digitizing image objects within a geographical information system environment (Archer et al., 1988; Ansley et al., 2001; Strand et al., 2006a); (*iii*) the use of propriety software such as Definiens Developer (Chubey et al., 2006); (*iv*) the application of one-dimensional (1D) and two-dimensional (2D) wavelets or other multiscale approaches to detect objects that exhibit a range of potential sizes (Burnett and Blaschke, 2003; Jordan and Schott, 2005; Strand et al., 2006a; Falkowski et al., 2006); (*v*) the application of methods such as Laplacian of Gaussian or textural filters that can detect object sizes relevant to a specifically chosen kernel size (Wang et al., 2004a; Hann et al., 2003); (*vi*) the application of a parcel-based classification when accurate, large-scale digital cartographic data are available (Aplin et al., 1999); and (*vii*) tree detection using valley-following approaches (Gougeon, 1995; Leckie et al., 2003b; 2005).

Over the last 5 years, there has also been a steady increase in the number of per-object image analysis studies in the peer-reviewed remote sensing literature that have applied commercial software packages. Many papers have used the Definiens Cognition Network Technology software, which was formerly known as eCognition (the most recent release of this software is called Definiens Developer). There are several commercial alternatives to Definiens, including the Feature Extraction Module offered by ITT Visual Information Systems for ENVI (Boulder, Colo.), Feature Analyst (Visual Learning Systems, Missoula, Mont.), and Infopack 2.0 (InfoSAR, Birkenhead, UK). A well-known free alternative is Spring 4.3.3 from Brazil's National Institute for Space Research (Camara et al., 1996).

Objects and the Definiens software

The Definiens software depends on image segmentation to create objects for classification (Baatz and Schäpe, 2000). The proprietary segmentation algorithm used by Definiens is usually referred to as "multiresolution segmentation," and it uses a bottom-up region merging approach to create the objects (Burnett and Blaschke, 2003). Starting at the pixel level, the values of pairs of neighboring pixels (in one or multiple image layers) are compared and then merged to form a single object if they satisfy a heterogeneity condition (Baatz and Schäpe, 2000; Burnett and Blaschke, 2003; Carleer et al., 2005). The heterogeneity condition is designed to minimize the average heterogeneity of object values across the image and maximize individual object homogeneity (Definiens, 2007). The pairwise comparison and merging process iterates, and object pairs are merged to create increasingly larger objects until a local homogeneity threshold is reached (Definiens, 2007). The course of the segmentation is user controlled through color and shape criteria that maximize within-object spectral homogeneity or across-scene object shape homogeneity, respectively.

When a single object level is created, the resulting image object contains spectral, shape, textural, neighborhood, and positional information (Definiens, 2007). The Definiens multispectral resolution algorithm permits the creation of

Vol. 34, Suppl. 2, 2008

multiple object layers, thus generating object hierarchies. Within an object hierarchy, objects on a lower level (subobjects) are nested within objects on an upper level (superobjects). When multiple object levels are present, objects also possess hierarchical information. The additional variables provided by the shape, textural, neighborhood, and hierarchical characteristics of the object add particular value to the classification procedure, especially in the case of panchromatic photographic imagery, which contains minimal spectral information.

In using multiresolution segmentation as part of a classification process, there are several issues that must be recognized (Wang et al., 2004b). Rarely expressed in the literature is the subjectivity of the user-defined Definiens software segmentation criteria, namely scale, color, and shape. When beginning a project, most analysts will apply the multiresolution segmentation algorithm in an exploratory fashion, simply trying different combinations of criteria until a satisfactory segmentation is achieved. The "rule of thumb" described by Definiens in their user guide (Definiens, 2007, p. 158) is to aim for a mean object size that is "as large as possible, yet small enough to show the contours of the structures that interest you." Baatz and Schäpe (2000) describe the user input into the process decisions as a historicity issue. Decisions made early on in the process will influence later decisions. Therefore, the segmentation is never fully reproducible. The historicity issue also raises challenges for the classification stage of the image analysis. An "unsatisfactory" segmentation can hinder effective classification of the object primitives

Objects and wavelet transformations

Another recent per-object method that has been used in remote sensing is that of applying 1D and 2D WTs to detect the location and size of image objects. The premise of most WT per-object methods is to identify the size of an image object by assuming that the dilation scale (i.e., the frequency or size of the wavelet) with the highest wavelet coefficient represents the specific object size (Jordan and Shott, 2005; Strand et al., 2006a; 2006b; 2008; Falkowski et al., 2006). Such analyses are inherently multiscale and enable the identification of objects across a range of sizes, provided they exhibit a shape that is similar to that of the wavelet mother function (Falkowski et al., 2006). One-dimensional examples of this and similar WT approaches have included the assessment of oceanic features (Wu and Liu, 2003), fault lines in topographic data (Jordan and Shott, 2005), analysis of canopy gaps (Bradshaw and Spies, 1992), and edges of rice fields (Ishida et al., 2004). Two-dimensional examples have included the identification of buildings within lidar data (Vu et al., 2003), measuring the crown widths of trees (Strand et al., 2006a; 2006b; 2008) and shrubs (Garrity et al., 2008) in aerial photography, and the quantification of the heights and crown widths of individual trees from lidar canopy height models (Falkowski et al., 2006; 2008).

Although the detection of 2D image objects within digital imagery remains relatively new to the remote sensing of vegetation at landscape scales (Falkowski et al., 2006; Strand et al., 2006a; 2006b; 2008), it is not a novel concept in the wider imaging literature. Medical imaging studies have used wavelet-based denoising and feature-enhancement methods since the mid-1990s to improve the visualization of microcalcifications in mammograms (Laine et al., 1994; Bruce and Adhami, 1999), an important early indicator of breast cancer (Addison, 2002). In fluid mechanics and meteorology, research has focused on the detection of cyclones and vortices within turbulent flows (Desrochers and Yee, 1999). In astronomy, such methods have been applied to assess spatial structure within microwave maps (Tenorio et al., 1999).

Methods

Study area

Readers are referred to Strand et al. (2006a; 2006b; 2008) for a full description of the study area and preparation of the aerial photography. The Owyhee Plateau extends over a 400 000 ha area in southwestern Idaho (43°N latitude, 116°W longitude). The area is characterized by western juniper woodlands (*Juniperus occidentalis* ssp. *occidentalis*) and sagebrush (*Artemisia* spp.) steppe. Other species present in low quantities are aspen (*Populus tremuloides*) and Douglas-fir (*Pseudotsuga mensiezii*). Western juniper in the study area occurs as open savanna-like woodlands at various stages of succession, ranging from old juniper woodlands commonly existing in rocky areas of fire refugium, to young woodlands, and to recently burned areas dominated by grasslands or sagebrush steppe. In terms of the topography, rocky canyons and riparian areas dissect the steppe and woodlands. The juniper occurs at approximately 1400–2560 m in elevation, with typical annual average precipitation ranging from 250 to 1000 mm across this elevation range. The expansion of western juniper into the steppe has been occurring for over 100 years and is believed to be a result of wildfire suppression, historic livestock grazing regimes, and fluctuations in precipitation patterns (Miller and Rose, 1995; Miller et al., 2005).

Panchromatic aerial photography at ~1 m spatial resolution was acquired for a portion of the Owyhee Plateau in southern Idaho in 1939 and 1998 (**Figure 2**). The historical 1 : 27 000 scale 1939 image was provided by the USDA-NRCS (1998) (formally Soil Conversation Service), and the 1998 digital orthophoto quarter quad (DOQQ) from the US Geological Survey (http://inside.uidaho.edu/geodata/USGS/DOQ.htm). The images were delivered as digital products scanned at 600 dpi. The 1998 orthophoto was orthorectified. The 1939 images were georeferenced to the 1998 image and clipped to identical spatial extents to allow comparisons of spatially identical areas. The root mean square area (RMSE) of the historical georeferenced photographs was ~10 m and was resampled to the ~1 m pixel size. Prior to analysis, each image was clipped to a 780 m × 600 m image in extent. This imagery and size were

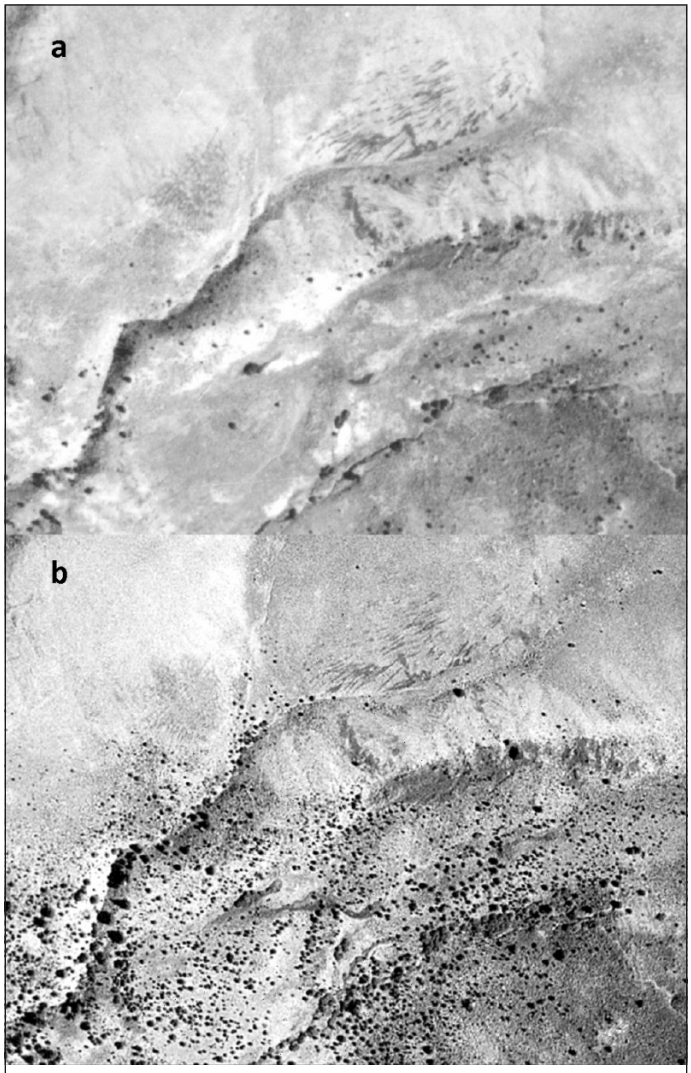

Figure 2. Aerial photographs of the study area for (a) 1939 and (b) 1998. Junipers appear as dark objects on a sagebrush-steppe background.

chosen because a range of juniper sizes was present and the total extent of the watershed of interest was included.

Production of per-object information by Definiens software

Definiens software was used to identify the location and size of individual juniper trees within the two images. In each case, three object levels were created (**Figure 3**). First, fine-scale segmentation was used to create a level of image object primitives that were smaller than the trees visible in the image (level 1). Then, a very coarse segmentation was applied to create an upper level of large superobjects (level 3). Lastly, an alternative algorithm, termed spectral difference segmentation, was used to refine the fine-resolution image object layer. Spectral difference segmentation is also a Definiens proprietary algorithm. It merges neighboring objects on the basis of spectral similarity, emphasizing spectral homogeneity at the expense of spatial uniformity in object size to produce a single level that contains multiscale objects (level 2).

In level 2, juniper objects are considerably smaller than most other nonjuniper objects within the scene (**Figure 3**), meaning that object area was very useful for juniper object classification. The segmentation procedure also resulted in a wide range of values of the mean difference to superobject, mean difference to scene, and mean difference to neighbors variables for level 2. The small, dark juniper objects usually had high values at the top of the range for each of the mean difference variables. The lighter nonjuniper objects had lower mean differences to superobjects, scene, and neighbors, regardless of size.

In total, five variables (object area, mean difference to superobjects, mean difference to scene, mean difference to neighbors, and mean object digital number) were combined in a logical AND statement to classify juniper objects within the scene (**Table 1**). For each image, training sample objects were selected (114 for 1939 and 164 for 1998), and a threshold value for each variable was determined with reference to the frequency distribution of values (**Table 1**). After classification, juniper objects were exported to ArcView (ESRI, Redlands, Calif.) shapefile format and then imported as a feature class into a file geodatabase. The file geodatabase automatically computes polygon area for its component feature classes. Polygons were subsequently converted to point (ArcTools: data management) to produce the marked point pattern of location and juniper area.

Production of per-object information by 2D WTs

As described elsewhere (Strand et al., 2006a; 2006b; 2008), 2D WTs were applied to the imagery to automatically estimate the location and crown widths of juniper trees. The 2D WT method or spatial wavelet analysis (SWA) operates by first producing a set of wavelet daughter functions $\{\Psi_{a,b}(x, y)\}$ (Jordan and Shott, 2005; Strand et al., 2006a; 2006b; 2008; Falkowski et al., 2006). The daughter functions are produced by changing the size and (x, y) position of the mother wavelet function $\{\Psi(x, y)\}$ via the following equation (Bruce et al., 2001; Addison, 2002):

$$\Psi_{a,b}(x, y) = \frac{1}{a}\Psi\left(\frac{\lambda - b}{a}\right) \quad (1)$$

where $a > 0$ is known as the dilation parameter and controls the width of each daughter function (Addison, 2002); the image location (x, y) of this function is given by λ; and the translation parameter b moves the location of the function across the image (Bruce and Li, 2001).

In traditional image processing, WT methods have been used to isolate and remove image noise by identifying which frequencies are associated with image anomalies. In contrast with taking the Fourier transform of the entire image, which can only provide information about the frequency or anomaly size, WT provides information on both the frequency and location of the image anomalies (Lindsay et al., 1996). The current methodology as applied by recent studies (Jordan and

Vol. 34, Suppl. 2, 2008

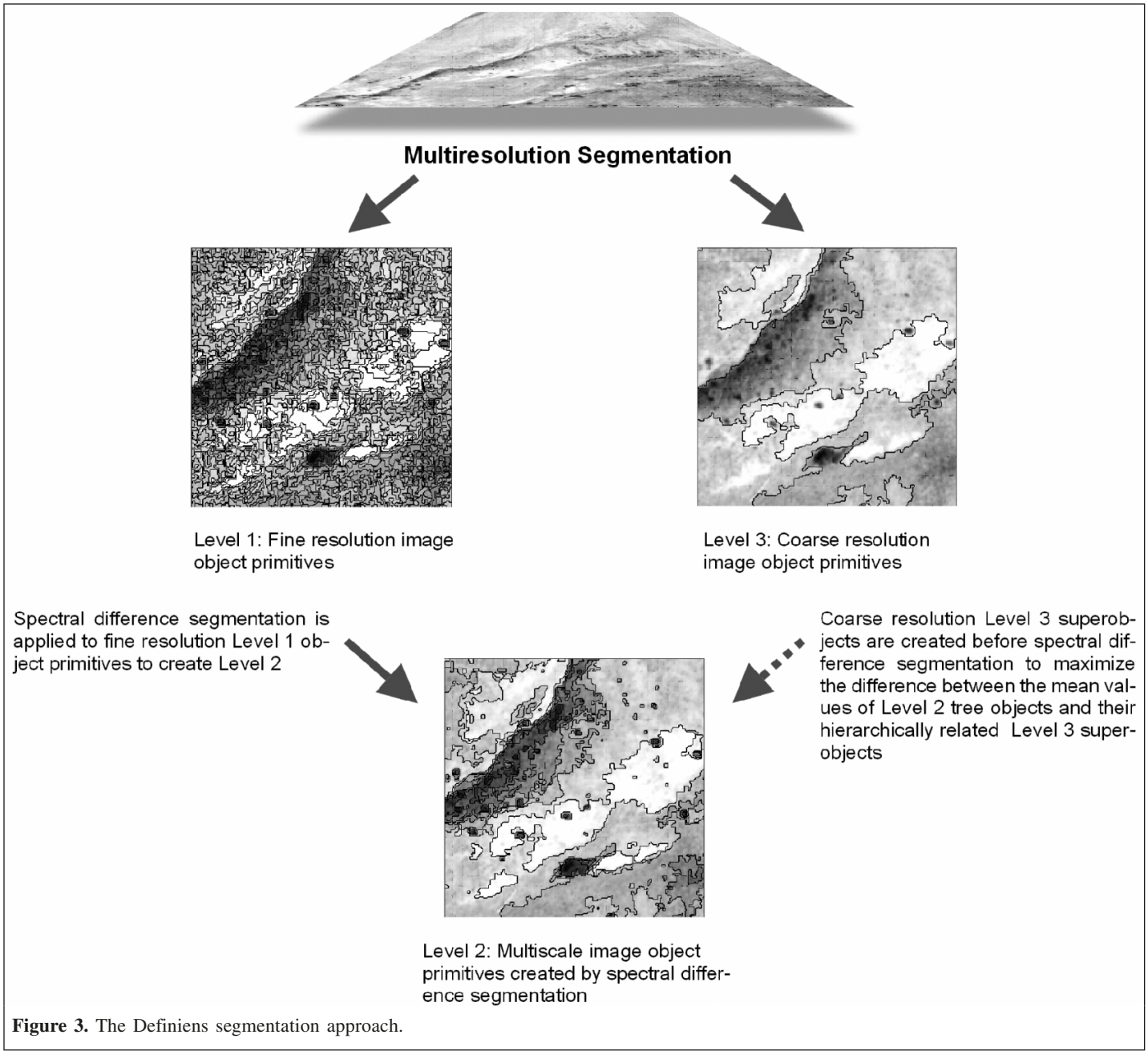

Figure 3. The Definiens segmentation approach.

Schott, 2005; Strand et al., 2006a; 2006b; 2008; Falkowski et al., 2006) uses the same information in a fundamentally different manner. Specifically, Jordan and Schott (2005) and Strand et al. (2006a; 2006b) both recognized that when analyzing image anomalies (or useful objects), the dilation scale with the highest wavelet coefficient could be assumed to correlate with the size of that object. Therefore, instead of identifying the location and size of the image anomalies for removal via a denoising procedure, the location and size of these objects are identified and the information retained for subsequent per-object analysis (Jordan and Schott, 2005; Strand et al., 2006a; 2006b).

Following Strand et al. (2006a; 2006b) and Falkowski et al. (2006), the Mexican Hat wavelet function was applied to the image data (**Figure 2**) over the range of likely tree radii (0–15 m, in increments of 0.1 m). In a manner similar to that of Jordan and Schott (2005), the methodology applied in this study is a discrete approximation to the continuous wavelet transformation. A 25-point local maximum identified the tree location. This process produces a marked point pattern image displaying the spatial location (x, y) and crown diameter (z) of each detected image object (i.e., juniper tree). When no juniper trees are detected at a location, the pixel is assigned a null value of –1. This methodology was applied to both datasets to produce a current and historical marked point pattern of individual juniper tree locations and crown diameters (**Figure 6**).

A schematic representation of the 2D WT approach is presented in **Figure 4**. The analysis of 1D time-varying signals

Table 1. Definiens software segmentation parameters for the 1939 and 1998 imagery.

	1939	1998
Segmentation parameters		
Multiresolution segmentation		
Level 1		
Scale	7	10
Composition of homogeneity criterion		
Color	0.95	
Shape	0.05	
Compactness	0.5	
Smoothness	0.5	
Level 3		
Scale	350	150
Composition of homogeneity criterion		
Color	0.95	
Shape	0.05	
Compactness	0.5	
Smoothness	0.5	
Spectral difference segmentation		
Level 2		
Spectral difference	14	18
Classification rules		
Variable thresholds for level 2 juniper objects		
Area	<51	<165
Mean object digital number (DN)	<116	<143
Mean difference to neighbors	< –9	< –9
Mean difference to scene	< –60	< –19
Mean difference to superobject	< –26	< –11

is typically achieved through the production of a frequency–time plot. For each location on the temporal axis (i.e., the abscissa, x), these plots highlight (red in **Figure 4**) which frequencies (i.e., daughter function dilation scales) are dominant within the original signal. Extension of this concept to two dimensions replaces the temporal axis, x, with two image coordinate axes, x and y, to produce a frequency–space image cube. For each (x, y) location, the daughter function dilation scale that best corresponds to the image feature at that given (x, y) location is highlighted. Selection of the daughter function scale responsible for the highest local maximum value over all the dilation scales is then determined by the wavelet coefficient. This indicates the highest correlation or goodness-of-fit between the specific wavelet daughter function shape (and dilation scale) and the image object (Falkowski et al., 2006). Determination of the local maximum of these WT values on the x, y plane provides the location of the object, with the size set by the identified dilation scale.

Production of spatial–structural change maps

Vegetation distribution maps were created by passing square moving windows (40 pixels × 40 pixels) over each marked point pattern image. Many moving window sizes could be compared, with perhaps adaptive windows used for mean and variance calculations. In terms of ecological data, the moving window size chosen will have further implications on the derived metrics (Turner et al., 2001). Similarly, arguments could be made for circular windows, given point dependence on seed dispersion (Strand et al., 2006b), or for other shapes. Analysis of optimal window size or shape is beyond the scope of this paper, as the optimal window will vary depending on the research questions asked and the management implications at hand.

In selecting an optimal window size, the challenge is to produce continuous maps (via a moving window) while retaining the spatially explicit information of the individual objects. These windows need to exhibit a sufficiently large window size such that an estimate of a given statistic is acquired. For example, the 40 pixel × 40 pixel window size was finally selected because it offered a balance between juniper sample size within each window and the ability to produce output "maps" that appeared continuous (and not too blocky in appearance). If the data are to be applied in process-modeling studies, we recommend following the methodologies outlined in numerous textural-analysis studies (Karathanassi et al., 2000; Keima, 2002; Coburn and Roberts, 2004) and investigate the most appropriate window size needed for the specific application. It is clear that the ideal window size will change with whatever process model you aim to parameterize as, for example, an ecological landscape succession model will operate on a scale different from that of a grass–tree interaction water budget model.

Standard distributional statistics (e.g., mean, minimum, maximum, count, skew, kurtosis, and standard deviation) were calculated within each moving window. These statistics only used the number and values of the marked point pattern values contained within each window. No null data were used in the calculation of the statistics. Each statistical value was then output to a new image. Change of the marked point pattern between 1939 and 1989 was quantified by differencing the individual spatial-statistics images. In a manner similar to that of temporal mixture analysis, where image "endmembers" are evaluated by identifying pixels that exhibit unique spectral properties over time (Piwowar et al., 1998; Piwowar, 2008), these differenced image layers highlight temporal (Δ) changes to a set (A) of spatial objects. In each of these cases, the number of samples used to calculate the statistic is the number of objects within the moving window and not the number of pixels.

Two clear analysis levels exist. In the first level, information is derived from the spatial locations of the marked point patterns and not through using any of the actual values associated with each point:

$$\Delta A(\text{population}) \rightarrow |\,\text{SUM}_f - \text{SUM}_i\,| \quad (2)$$

$$\Delta A(\text{dispersion}) \rightarrow |\,\text{KDE}_f - \text{KDE}_i\,| \quad (3)$$

where the subscripts f and i denote current and historical data, respectively; SUM denotes the total number of trees within the 40 pixel × 40 pixel moving window, and the change in SUM between current and historical marked point patterns of trees in a landscape can be considered to highlight a change in

Vol. 34, Suppl. 2, 2008

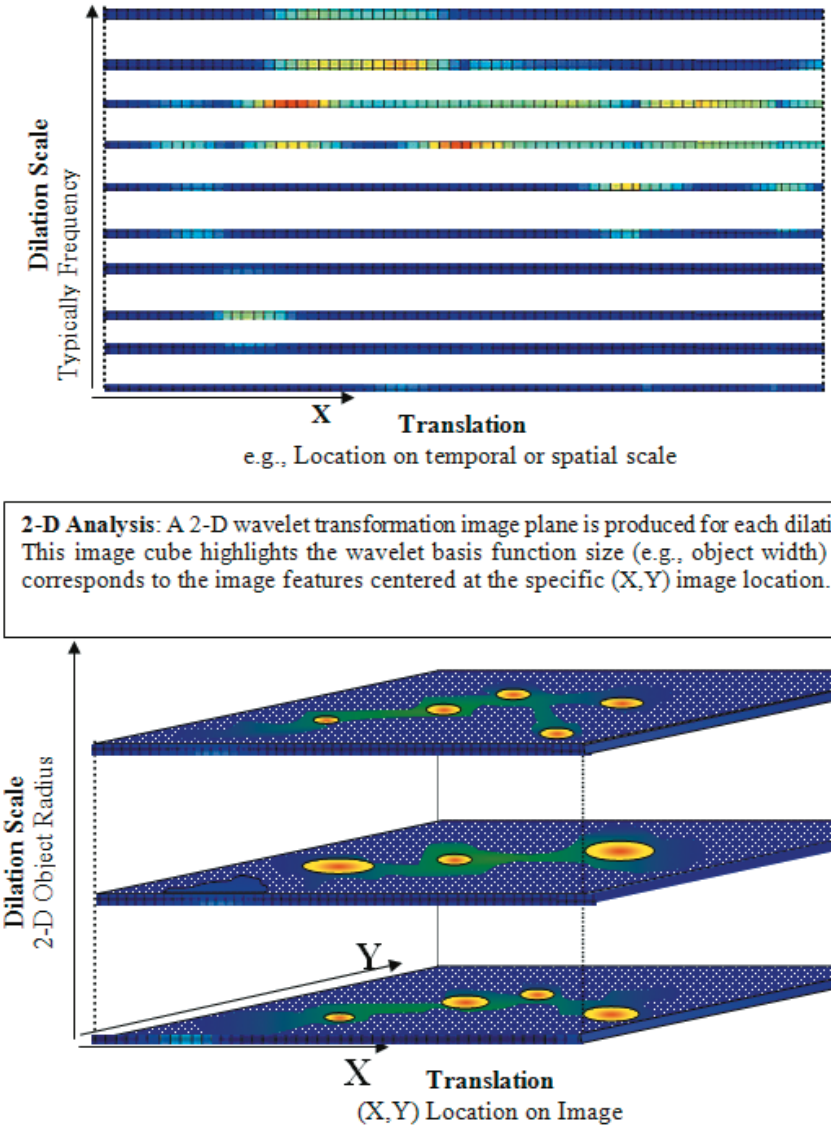

Figure 4. Spatial wavelet analysis (SWA) approach (adapted from Falkowski et al., 2006).

population (**Figure 7**); and KDE refers to the kernel density estimate statistic, which provides a measure of how the points are distributed spatially (**Figure 10**). This latter measure considers the spatial interdispersion (e.g., clumped or spread out) or the clustering and diffusion of the points within the extent of the moving window. The KDE surfaces were derived using a standard univariate 2D moving window probability KDE using a 200 m search window with the juniper diameters as the weighting variable.

The application of point pattern statistics enables analysis of the spatial and temporal change in juniper distribution based on an empirical spatial model. The juniper crown diameter estimates were analyzed using marked point pattern, local statistic Gi* (Getis and Ord, 1992), and nearest neighbor NN (Boots and Geits, 1988) statistics. These statistics were selected to identify the change of dispersal of junipers between 1939 and 1998. The Gi* is a measure of global spatial association at different distance lags (bandwidths) and is often used to indicate clustering, dispersal, or complete spatial randomness (CSR). The Gi* is a local statistic that is defined as the difference in the sample and weighted global mean divided by the weighted global standard deviation (Lee and Rogerson, 2007). The significance of the statistic is reported as a z score. The Gi* statistic highlights clusters that have values significantly greater than or lower than the global mean (Laffan, 2002). The Gi* value, $G(d)$, is zero when no clustering

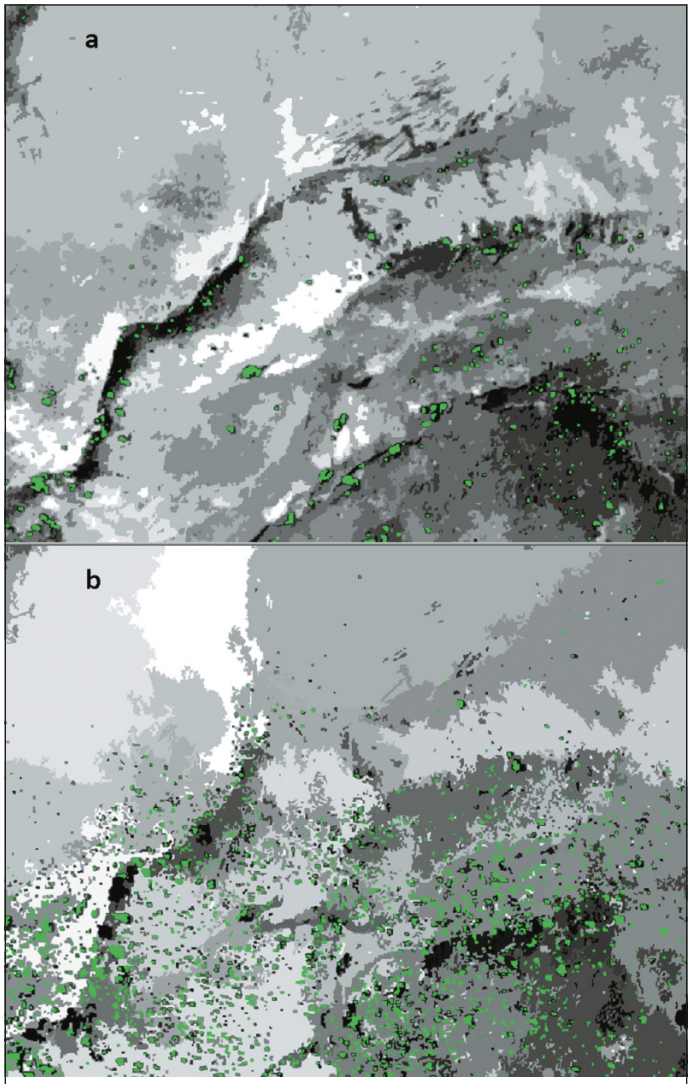

Figure 5. Output of the Definiens software presented for (a) 1939 and (b) 1998. Segmentation of the landscape is presented as both contiguous areas (grey scale) and final per-object tree polygon outputs (green overlay).

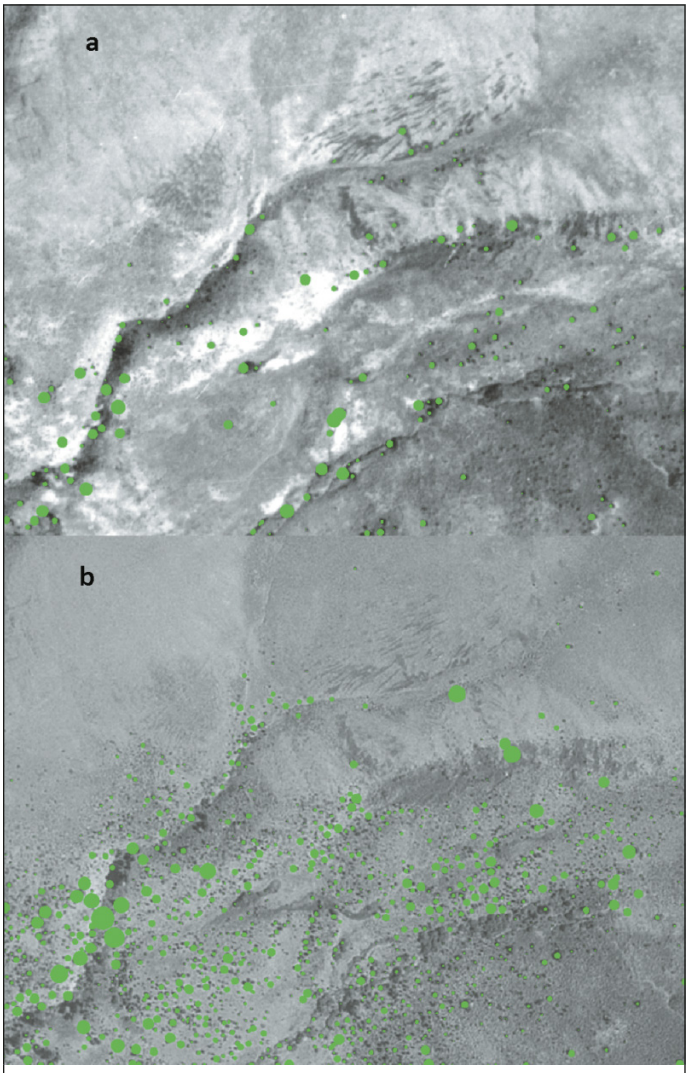

Figure 6. Output of the 2D wavelet transformation per-object method presented by green overlays for (a) 1939 and (b) 1998 (adapted from Strand et al., 2006a; 2006b).

is apparent, is positive when the cluster exceeds the global mean, and becomes increasingly positive with greater clustering (Laffan, 2002).

We used 10 m distance bandwidths with 10 m increments and a maximum distance of 200 m to calculate Gi* in R (R Development Core Team, 2007) using the package spdep v.0.4-13 (Bivand, 2007). NN analysis was used to examine the distance of *n*-order neighbors (we addressed first-order neighbors) and then compare it with expected values for a random sample of points from a CSR pattern (Diggle, 2003).

In the second level, information is derived from analyzing the distributions of the values from each point (i.e., crown sizes in this case) within the extent of the moving window. For example, a change in mean crown widths (or tree heights if lidar) can highlight a change in growth or biomass and carbon (**Figure 8**) (Strand et al., 2008); and a change in standard deviation, skew, or kurtosis can be thought to highlight changes in the relative number of large and small objects within the moving window, which may indicate processes of succession (**Figure 9**):

$$\Delta A(\text{growth}) \rightarrow |\,\text{MEAN}_f - \text{MEAN}_i\,| \quad (4)$$

$$\Delta A(\text{association}) \rightarrow |\,\text{STDEV}_f - \text{STDEV}_i\,| \quad (5a)$$

$$\rightarrow |\,\text{Skew}_f - \text{Skew}_i\,| \quad (5b)$$

$$\rightarrow |\,\text{Kurtosis}_f - \text{Kurtosis}_i\,| \quad (5c)$$

where the subscripts f and i denote current and historical data, respectively; and MEAN and STDEV denote the mean and standard deviation, respectively, of the tree crown widths within the 40 pixel × 40 pixel moving window. The maps of standard deviation, skew, or kurtosis are described by the term

Vol. 34, Suppl. 2, 2008

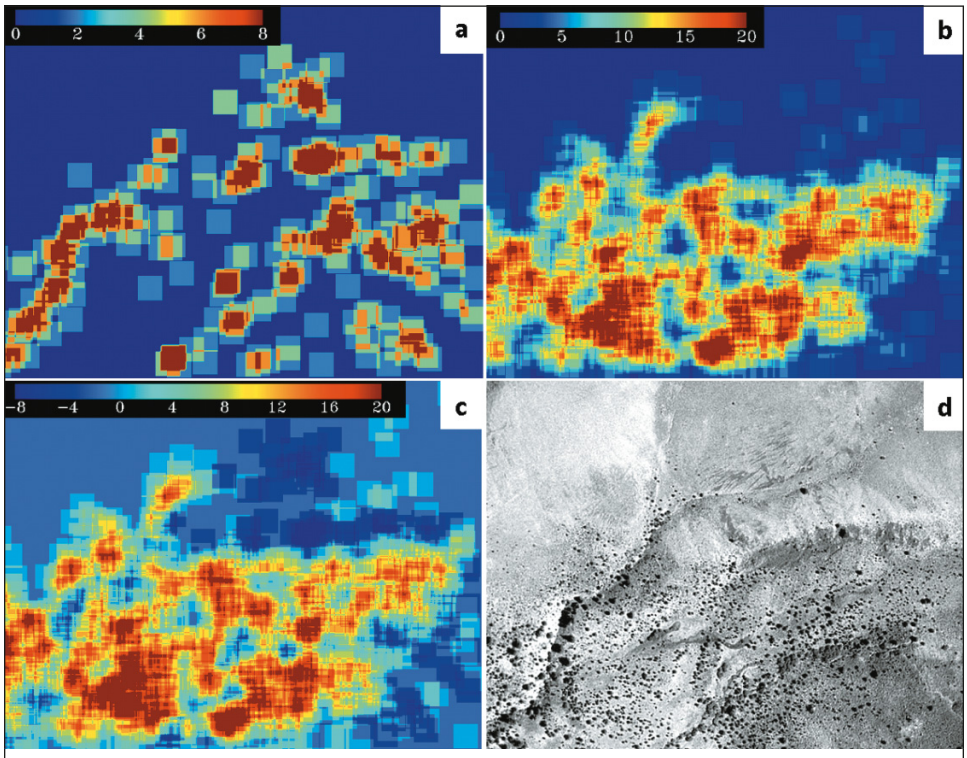

Figure 7. Juniper population maps derived by counting all juniper objects within the 40 pixel × 40 pixel moving window. (a) Spatial distribution of juniper population in 1939. (b) Spatial distribution of juniper population in 1998. (c) Spatial–temporal changes in juniper population between 1939 and 1998. (d) Aerial photograph from 1998 included to aid comparison. Units in images (a)–(c) are a count of the number of junipers per window size.

association, as the statistics do not include spatial information of where within the moving window the large and small objects are, but rather only the relative quantity or association of large to small object sizes. To derive the initial and final statistical size distributions, any dataset of comparable spatial resolution could be used (e.g., current lidar and historic aerial photographs), and therefore the production of the final ΔA could be considered as a data integration process. As the output of each per-object method is an absolute metric (e.g., object width in metres derived from pixel size × object width), having comparable spatial resolutions (e.g., 1 m and 2.4 m) makes it more likely that objects of similar spatial size will be detected. Using data of 1 m and 30 m spatial resolution may detect objects in each case, but it will be unlikely that the objects in each image present the same phenomena.

Results and discussion

General landscape changes

The new images created for 1939 and 1998 revealed several spatially continuous properties of vegetation stand structure and distribution occurring across the landscape. In 1939, the landscape was sparsely populated with juniper trees, and they appeared to primarily occur within draws and were clustered as small islands or refugia (Camp et al., 1997). These trees were relatively diverse in terms of crown width (**Figure 8a**). Overall, the crown width distribution was relatively neutral in skew, with localized areas of either positive or negative skew (**Figure 9c**).

Analysis of the 1998 images revealed that the trees were more evenly spread across the landscape rather than being clumped in isolated patches. Overall, mean tree crown width was homogeneous, suggesting that many of the trees were relatively even in size and likely also in age (**Figure 8b**). This analysis is consistent with the fact that fire suppression has been actively practiced in this region, allowing juniper to spread into areas in which they were previously absent. Additionally, much of the area was dominated by regions that had a positive skew in tree crown width distribution (i.e., dominated by smaller trees), and there were fewer areas with a negatively skewed distribution (i.e., dominated by larger trees) in crown width when compared with the 1939 data (**Figure 9d**). This also suggests that lack of fire has allowed juniper seed, originating from the large trees observed in the 1939 photography, to spread, germinate, and establish a new cohort of young juniper plants across the landscape.

WT and Definiens software comparison

The Definiens segmentation and classification procedure is supervised by the user input and as such is affected by the

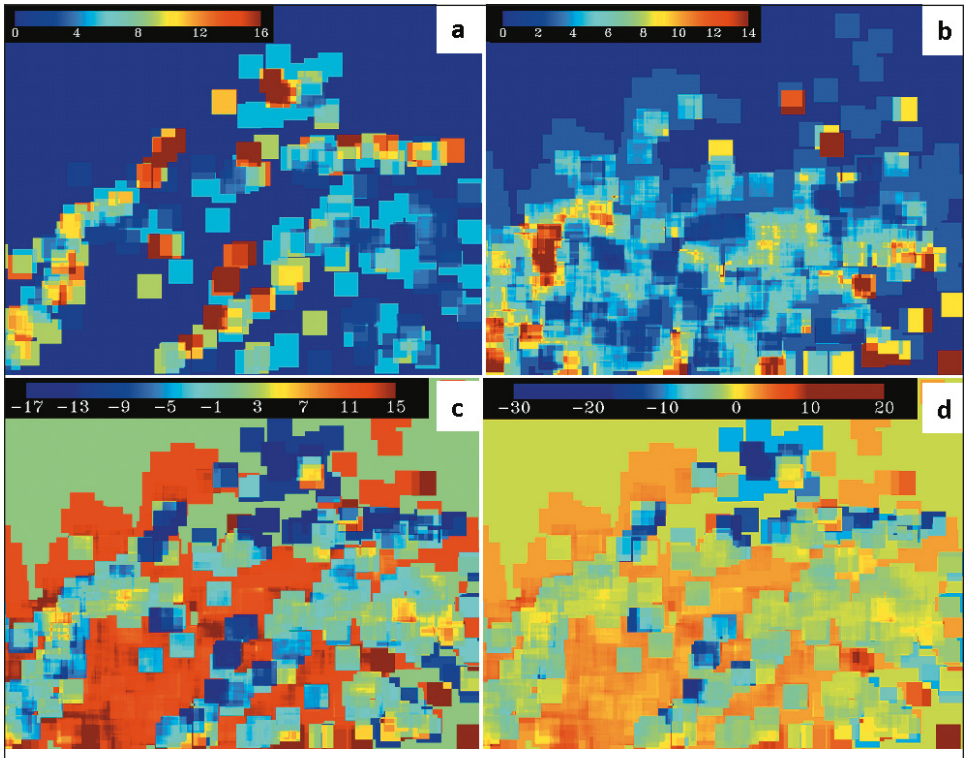

Figure 8. Juniper growth or biomass maps derived by calculating the mean crown width of all juniper objects within the 40 pixel × 40 pixel moving window. (a) Spatial distribution of juniper crown widths in 1939. (b) Spatial distribution of juniper crown widths in 1998. (c) Spatial–temporal changes in juniper crown widths between 1939 and 1998. (d) Foliar biomass change (kg) between 1939 and 1998 using allometric relations of Gholz et al. (1979) as presented in Ter-Mikaelian and Korsukhin (1997). Units in images (a)–(c) are average juniper crown width in metres per 40 pixel × 40 pixel window.

subjectivity of the user's decisions. Within the remote sensing literature, few papers have acknowledged the issue of how to achieve optimal segmentation of an image (Addink et al., 2007). Most published remote sensing research depends on the user's visual analysis of segmentation results, but there are many papers from the pattern recognition and computer vision literature that offer objective methods for evaluating segmentation (e.g., Zhang and Gerbrands, 1994; Zhang, 1996, 1997; Zhang et al., 2008). Carleer et al. (2005) reviewed these methods and demonstrated how so-called "empirical discrepancy evaluation methods" could be used to analyze segmentation of IKONOS imagery. Ideally, this kind of quantitative evaluation should be incorporated in any per-object-based analyses that involve image segmentation.

The Definiens segmentation procedure permits the creation of multiple layers of objects, therefore allowing the analyses and classification of objects at multiple scales. The limitations to any analysis are generally defined by the expertise of the user and the time available to perfect a multiscale analysis. For the current research, the spectral difference algorithm was used to create objects of multiple scales on a single object level in the hierarchy. This approach was satisfactory for a demonstration of the method, but visual assessment of **Figures 2** and **5** reveals a slight oversegmentation of larger juniper objects and undersegmentation of smaller juniper objects. Oversegmentation is not as serious a problem as undersegmentation because it can be rectified after classification (Carleer et al., 2005). Undersegmentation most commonly results in misclassification of image objects. For example, in this study, undersegmentation of smaller juniper objects meant that they were merged with background objects and omitted from the juniper class.

Another issue associated with the segmentation stage of the analysis is that for larger trees there was separation of the individual juniper canopy into sunlit and shaded portions. This issue feeds into the historicity aspect of the segmentation and classification process. Where a tree canopy is segmented into spectrally different objects, it is usually necessary to compensate for this in the classification process. This can be achieved by adding an OR statement or by using class-related features where sunlit canopy objects are classified according to their proximity to shaded canopy objects. In a handful of cases, the segmentation procedure failed to separate sunlit canopy from background objects. This could be rectified with increasing the degree of oversegmentation of the image. In either case, if the difference in illumination across the canopy is not accounted for, then the Definiens-based method can result in underestimation of canopy size.

Vol. 34, Suppl. 2, 2008

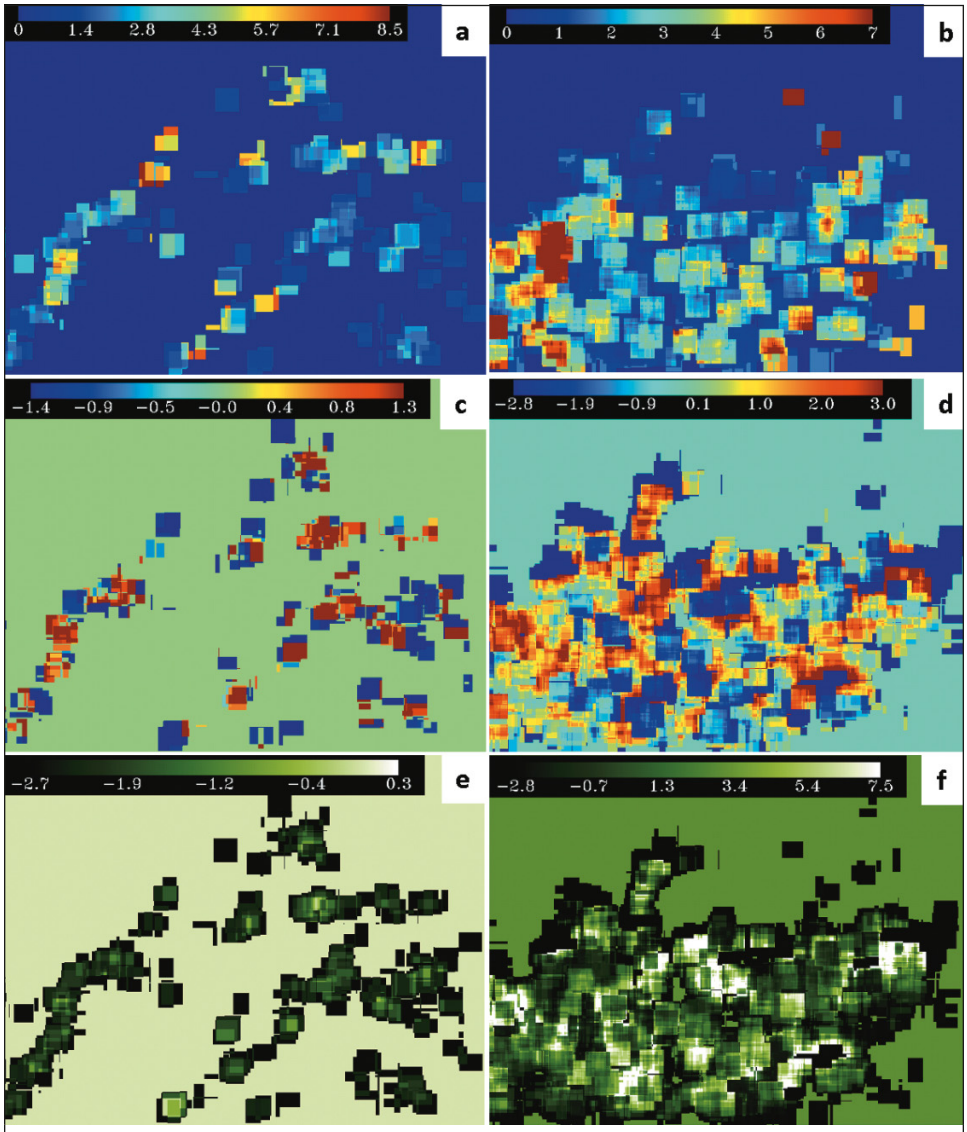

Figure 9. Juniper size association maps by calculating the standard deviation (a, b), skew (c, d), and kurtosis (e, f) within the 40 pixel × 40 pixel moving windows. (a, c, e) Spatial distribution of statistics in 1939. (b, d, f) Spatial distribution of statistics in 1998.

Problems associated with classification of tree objects mainly arose from the lack of spectral information in the panchromatic aerial photograph imagery and the low contrast of the imagery. Using the combination of additional variables created by the segmentation process and the image digital numbers greatly assisted in classifying juniper objects. However, even when thresholds are defined for juniper and nonjuniper objects over a range of variables, there are still some nonjuniper objects that fulfill the minimum classification criteria for juniper and are therefore misclassified. On closer examination of the imagery, the misclassified objects were most often darker patches of grass or forbs or possibly sagebrush. Conversely, there were small trees that were missed by the classification rule. These were mostly omitted because the mean object digital number threshold was set too low. Increasing this threshold resulted in more errors of commission involving dark grass–forb patches. Over a limited area such as the study site selected for this research, it is possible to correct misclassified objects by hand. Of course, this would not be feasible for practical applications over large areas. The simple additive threshold classification rule performed adequately for this paper, but it would be advisable to consider a more involved segmentation approach and classification of juniper and nonjuniper objects over several object levels to improve the accuracy of juniper extraction from panchromatic photographic imagery.

Lastly, the last challenge to the use of Definiens software to extract juniper is the export of juniper objects and the creation of a marked point layer. After classification, juniper objects were merged so that a single object represented a single tree. However, where the canopies of several trees overlap, the merge process created a single object for several trees. This

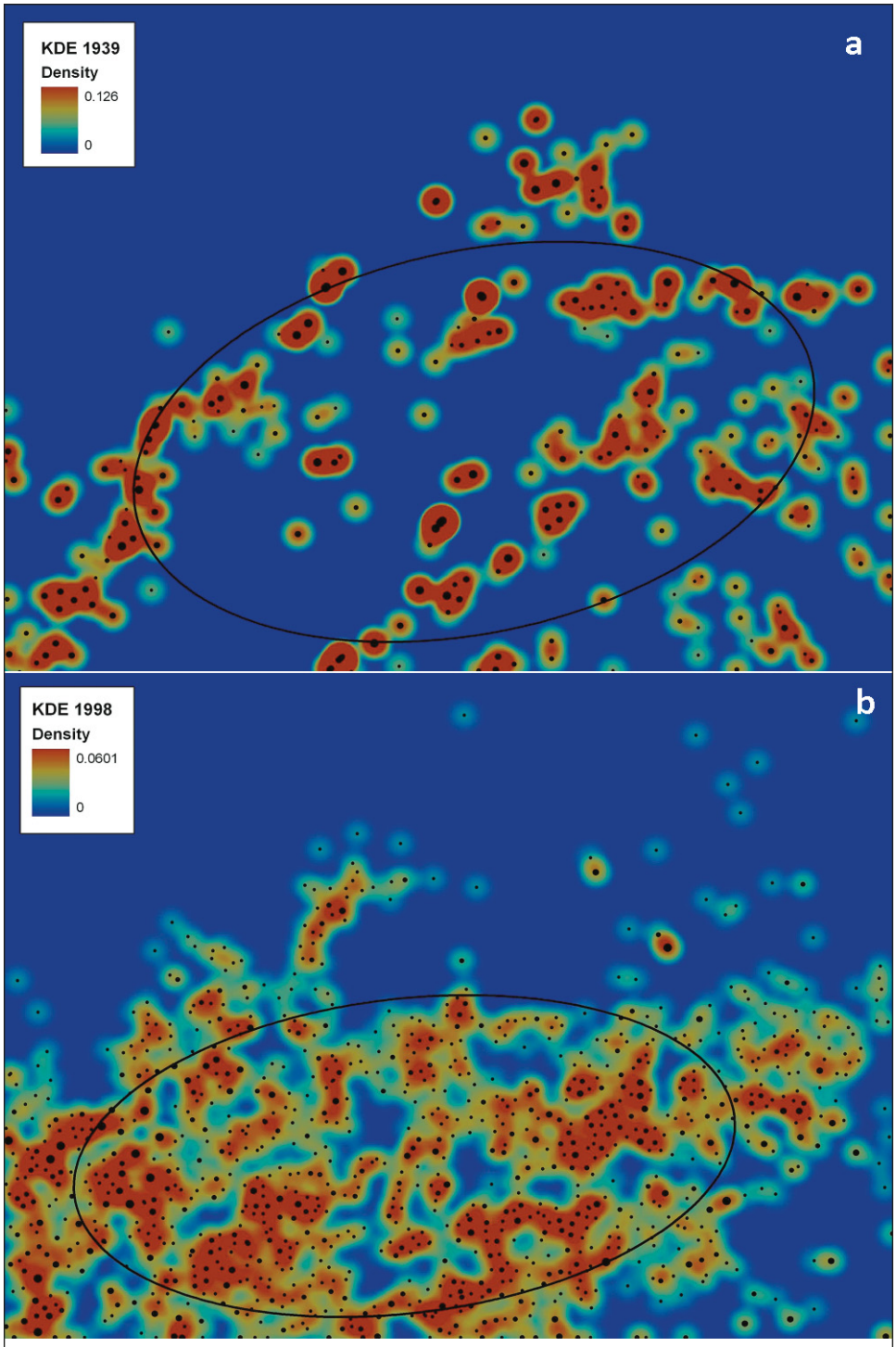

Figure 10. Juniper clustering and diffusion maps produced using marked point pattern statistics.

error was carried forward in the creation of the point layer where a single point replaced the polygon in representing a group of trees.

Despite the sampling framework imposed by the scale of the photographs and the resolution at which they were scanned and resampled to, the Definiens segmentation procedure does appear to provide a more accurate rendition of the juniper canopy clumps (i.e., where the crowns merge) than the WT method. This is mainly because the WT method assumes a circular canopy shape, which is an approximation. The bottom right of **Figures 2b**, **5b**, and **6b** illustrates that there are places where Definiens picks up trees that the WT method missed. This is likely due to the WT method's minimum detection size of about two to three image pixels in width (Strand et al.,

2006a; 2006b; 2008). In a similar manner, WT methods have shown that this method is optimally suited in open canopy woodlands and is not appropriate when crown closure exceeds 55% (Strand et al., 2008; Falkowski et al., 2008). However, from a carbon accounting standpoint, Strand et al. (2008) highlighted that the 2D WT method was able to characterize 96% of the aboveground foliar carbon in these open canopy juniper woodlands.

Although the Definiens segmentation procedure provides more accurate merged crown shapes and identifies the smaller juniper plants, its subjectivity, lack of result reproducibility, and time-consuming aspect (i.e., multiple steps are needed to get to the same end result) make the WT method a more attractive approach for large-scale assessment of trees in these open canopy woodlands. The typical total computation time of the WT method for imagery this size is ~2 min; by comparison, the total Definiens segmentation procedure took almost 2 h to finalize for each image. Determining which variables to use in the classification and setting appropriate thresholds for the classification rule took another 2 h per image. As evident in **Figures 5** and **6** and also observed in prior studies (Strand et al., 2006a; 2006b; 2008), both methods are apparently insensitive to the tone of the background in that dark objects are detected on both the light and dark backgrounds. The WT method has also been shown to work well on structurally smaller shrubs (Garrity et al., 2008) but is limited when shadow lengths make the total object shapes appear elliptical (S.R. Garrity, unpublished data).

Strand et al. (2006a; 2006b) further reported the accuracy of the WT method applied to a subset of the 1998 imagery (**Figure 6b**) to be 81%, with 8% omission and 5% commission errors. In the current study, the 1998 image was reassessed, and the Definiens software output (**Figure 5b**) obtained an overall accuracy of 95%, but with a 25% commission error (**Table 2**). These results illustrate that, although the simple segmentation and classification method using the Definiens software can detect juniper image objects, it appears less able to discriminate between the types of image object, whereas the WT method is optimally suited to detect juniper trees because their crowns are generally circular in shape and exhibit a range of characteristic sizes. The total percent juniper cover produced was also assessed for **Figures 5** and **6**. In the 1939 imagery, the percent juniper cover was 1.2% (WT) and 0.06% (Definiens software), whereas in the 1998 imagery the percent juniper cover was 4.4% (WT) and 3.5% (Definiens software). From a wider study in the same environment, Strand et al. (2008) compared the WT estimate of percent juniper cover with field data and determined that the WT underestimated the cover by ~23%. Therefore, extending these prior results to this study suggests that Definiens software will likely further underestimate the actual juniper cover. Comparing these per-object-based results with the conclusions of Strand et al. (2008), where a per-pixel texture-based assessment produced an overestimation of cover of 180%, highlights that either per-object method provides an improved estimate of percent juniper cover.

Table 2. Definiens software accuracy assessment for the 1998 imagery.

				Accuracy (%)	
	Trees	Not trees	Total	Producers	Users
Trees	581	146	727	76.3	79.9
Not trees	180	5252	5431	97.3	96.7
Total	761	5398	6158	Overall accuracy = 94.7%	

Object population maps

To obtain a magnitude of the juniper population in both 1939 and 1998 and thus the population change, the sum of each individuals object (given by the occurrence of a location and not using the derived metrics) within the extent of the moving window was calculated (**Figure 7**). Although **Figure 7** represents the output of the 2D WT per-object method, the location, and thus occurrence, of individual image objects can realistically be obtained by most per-object approaches. Comparison of **Figure 2** with **Figures 7a–7c** shows that this simple statistic can discriminate across the range of population conditions from juniper decline, through static populations, to areas that have seen considerable population expansion. The juniper Δ population map (**Figure 7c**) highlights the juniper expansion from the valleys in 1939 to across the plateaus in 1998.

Object growth maps

Application of per-object methods to characterize per-object size information such as crown width, crown area, or even tree height if lidar data are employed can enable the production of quantitative maps of growth or decline in productivity and biomass. In the case of the juniper aerial photography example employed in this study, where allometric relationships between crown width and aboveground biomass have been presented in prior studies (Strand et al., 2008), **Figure 8c** represents the change in aboveground juniper carbon from 1939 to 1998. Equally, such maps produced using lidar could spatially describe the growth of trees via depicting temporal changes in maximum tree height in addition to crown widths (Falkowski et al., 2006), or even inferred characteristics such as basal area (Hudak et al., 2006) or diameter at breast height (Anderson et al., 2005), which are important metrics in forestry.

Association of object size (or woodland development) maps

We propose that the standard deviation, skew, and kurtosis of the crown width distributions each contribute to describing the structure of the juniper stands within this environment. The development of western juniper woodlands in areas that were previously dominated by shrub steppe has been classified into four phases, phases I–III and mature woodlands (Miller et al., 2005). This classification is widely used in management of

pinyon–juniper woodlands. Phase I represents the initiation phase of woodland development and is characterized by low juniper cover (<10% of the potential cover for the site) where shrub steppe vegetation is still dominant and the ecological processes (e.g., hydrology, fire regimes, nutrient cycling) have not yet been influenced by the presence of juniper plants on the site. A point pattern in phase I, derived from object-oriented remote sensing methods such as those described in this paper, would be characterized by a low mean number of plants (few juniper plants), a low mean crown diameter, a low standard deviation (most plants are small with little variation in size), and a positive skew because most plants are small. In phase II, the juniper component is codominant with the shrub steppe vegetation, ecological processes are being altered, and the juniper cover is 10%–30% of the potential for the site. The older trees within the stand are beginning to produce seed, resulting in recruitment of young juniper seedlings in the interspaces of the older trees and an increase in woodland density and juniper cover.

A point pattern derived during phase II would be characterized by a larger number of juniper plants, resulting in a higher mean than in phase I. The standard deviation would be higher because there are juniper trees of several different sizes, and the skew would be less positive than that for phase I. In phase III of juniper woodland development, the trees form the dominant vegetation, and the canopy cover is approaching the potential for the site. The number of trees and the size of the trees have increased compared with phases I and II, resulting in a point pattern with a higher mean number of trees (higher tree density), higher mean crown diameter, higher standard deviation (variable sizes of trees), and less positive skew than in either phase I or phase II. Similarly, the mature woodland stage would be characterized by a distribution with a negative crown width skew representing those conditions with several large junipers but very few small junipers, or if they are present they are below the particular method detection limit (2 m for 2D wavelet transformations). **Figures 9c** and **9d** depict how the skew of crown widths changes across the juniper landscape. Through a combination of the mean crown width, standard deviation, and skew, the structural development stage of woodlands could be mapped at a level of detail that is useful in land management.

Object dispersion maps and point pattern analysis

The point pattern analysis and presentation of the kernel density estimator are shown in **Figure 7**. The z score in the 1939 data indicates significant clustering at 20 m (z score = 2.4597) with a lower than expected $G(d)$ value (observed $G(d)$ of 0.0071 versus expected $G(d)$ of 0.0064), indicating high clustering of small diameters. The nearest-neighbor statistic indicates an average stem density of 19.8 m. In contrast, the 1998 results are strongly supported at 120 m (z score = 1.0377), with the $G(d)$ value of 0.14 equal to the expected value, indicating clustering of mixed stem diameters. However, the nearest-neighbor distance increases (10.5 m). The results demonstrate a weakening in the autocorrelation between 1939 and 1998, indicating a diffusion (spread) of juniper while exhibiting a two-fold increase in the stem density.

Conclusions

This study compared the per-object characterization ability of two contemporary methods. The results demonstrate that, although the user can eventually produce a reasonable collection of objects (e.g., 95% accuracy with 25% commission error) using Definiens software, the approach is subjective and that, more importantly, the precise decisions used to produce the segmentation may not be easily repeatable. In contrast, the wavelet transformations (WTs) methodology is less likely to identify incorrect objects (5% commission error) and is repeatable, but it exhibits a lower accuracy (81%).

This study also used per-object data of individual tree locations and sizes to create new, spatially continuous data layers quantifying the spatial distribution of vegetation structure across time. These new data layers represent a step forward in the extraction of inherent image information, beyond the analysis of statistical moments (intensity, variance, skew, etc.) traditionally applied in per-pixel remote sensing analysis of panchromatic digital imagery. Although several basic statistics (including sum of trees, mean crown width, standard deviation, and the level of skew of the crown width) and point pattern statistics were applied, the possibilities for statistical calculations are not restricted. These new data layers have the potential to provide valuable information, as they can be incorporated into land-cover classifications and various biophysical models attempting to explain or predict ecosystem processes and functions. Their application as a tool for studying vegetation will certainly provide valuable information for studies concerning spatial patterns of plant invasion, dispersal, disturbance, carbon storage, stand mapping, and successional development. Ultimately, these new spatial–structural data layers allow for the continuous analysis of both contemporary and historical conditions, which when coupled could further our ability to predict and model natural processes and future impact of management practices on the environment.

This study demonstrates that relatively low technology remotely sensed data (i.e., historical aerial photographs) can be used to obtain vital quantitative measures of vegetation structure and arrangement across broad spatial scales. These new information layers of population, growth, association, and dispersion are essentially inherent image properties relevant to all per-object remote sensing applications. Building on the light detection and ranging (lidar) study of Vu et al. (2003), such data could equally refer to changes in urban development, where population refers to the number of buildings, growth to the relative or average size of buildings, and association to the ratio of the number of large warehouses to, for example, the number of residential homes.

Vol. 34, Suppl. 2, 2008

Acknowledgements

The research was in part supported by the Forest Public Access Resource Center (ForestPARC), the Upper Midwest Aerospace Consortium (UMAC), which is in turn funded by the National Aeronautics and Space Administration (NASA).

References

Addink, E.A., de Jong, S.M., and Pebesma, E.J. 2007. The importance of scale in object-based mapping of vegetation parameters with hyperspectral imagery. *Photogrammetric Engineering & Remote Sensing*, Vol. 73, No. 8, pp. 905–912.

Addison, P.S. 2002. *The illustrated wavelet transform handbook*. Institute of Physics Publishing, The Institute of Physics, London, UK. 143 pp.

Anderson, H.-E., McHaughey, R.J., and Reutebuch, S.E. 2005. Estimating forest canopy fuel parameters using LIDAR data. *Remote Sensing of Environment*, Vol. 99, pp. 441–449.

Ansley, R.J., Wu, X.B., and Kramp, B.A. 2001. Observation: long-term increase in mesquite canopy cover in a north Texas savanna. *Journal of Range Management*, Vol. 54, pp. 171–176.

Aplin, P., Atkinson, P.M., and Curran, P.J. 1999. Fine spatial resolution simulated satellite sensor imagery for land cover mapping in the United Kingdom. *Remote Sensing of Environment*, Vol. 68, pp. 206–216.

Archer, S., Scifres, C.J., Bassham, C.R., and Maggio, R. 1988. Autogenic succession in a subtropical savanna: conversion of grassland to thorn woodland. *Ecological Monographs*, Vol. 58, pp. 111–127.

Asner, G.P., Archer, S., Hughes, R.F., Ansley, R.J., and Wessman, C.A. 2003. Net change in regional woody vegetation cover and carbon storage in Texas drylands, 1937–1999. *Global Change Biology*, Vol. 9, pp. 316–335.

Atkinson, P.M., and Lewis, P. 2000. Geostatistical classification for remote sensing: an introduction. *Computers and Geosciences*, Vol. 26, pp. 361–371.

Baatz, M., and Schäpe, A. 2000. Multiresolution segmentation — an optimization approach for high quality multi-scale image segmentation. In *Angewandte Geographische Informationsverarbeitung XII*. Edited by J. Strobl, T. Blaschke, and G. Griesebner. G. Wichmann-Verlag, Heidelberg, Germany. pp. 12–23.

Berberoglu, S., Lloyd, C.D., Atkinson, P.M., and Curran, P.J. 2000. The integration of spectral and textural information using neural networks for land cover mapping in the Mediterranean. *Computers and Geosciences*, Vol. 26, No. 4, pp. 385–396.

Berberoglu, S., Curran, P.J., Lloyd, C.D., and Atkinson, P.M. 2007. Texture classification of Mediterranean land cover. *International Journal of Applied Earth Observation and Geoinformation*, Vol. 9, pp. 322–334.

Bivand, R. 2007. *Package spdep — spatial dependence: weighting schemes, statistics and models*. R package, version 0.4-12.

Boots, B.N., and Getis, A. 1988. *Point pattern analysis*. Sage Publications, Newbury Park, Calif.

Bradshaw, G.A., and Spies, T.A. 1992. Characterizing canopy gap structure in forests using wavelet analysis. *Journal of Ecology*, Vol. 80, pp. 205–215.

Bruce, L.M., and Adhami, R.R. 1999. Classifying mammographic mass shapes using the wavelet transform modulus-maxima method. *IEEE Transactions on Medical Imaging*, Vol. 18, No. 12, pp. 1170–1177.

Bruce, L.M., and Li, J. 2001. Wavelets for computationally efficient hyperspectral derivative analysis. *IEEE Transactions on Geoscience and Remote Sensing*, Vol. 39, No. 7, pp. 1540–1546.

Bruce, L.M., Morgan, C., and Larsen, S. 2001. Automated detection of subpixel hyperspectral targets with continuous and discrete wavelet transforms. *IEEE Transactions on Geoscience and Remote Sensing*, Vol. 39, No. 10, pp. 2217–2226.

~~Bunting, S.C., Strand, E.K., and Kingery, J.L. 2007. Landscape characteristics of sagebrush-steppe/juniper woodland mosaics under varying modeled prescribed fire regimes. In *Proceedings of the 23rd Tall Timbers Fire Ecology Conference: Fire in Grassland and Shrubland Ecosystems*. Edited by R.E. Masters and K.E.M. Galley. Tall Timbers Research Station, Tallahassee, Fla. pp. 50–57.~~

Burnett, C., and Blaschke, T. 2003. A multi-scale segmentation/object relationship modelling methodology for landscape analysis. *Ecological Modelling*, Vol. 168, pp. 233–249.

Camara, G., Freitas, R.C.M., Souza, U.M., and Garrido, J. 1996. SPRING: Integrating remote sensing and GIS by object-oriented data modeling. *Computers & Graphics*, Vol. 20, No. 3, pp. 395–403.

Camp, A.E., Hessburg, P.F., Everett, R.L., and Oliver, C.D. 1997. Predicting late-successional fire refugia pre-dating European settlement in the Wenatchee Mountains. *Forest Ecology and Management*, Vol. 95, pp. 63–77.

Carleer, A.P., Debeir, O., and Wolff, E. 2005. Assessment of very high resolution satellite image segmentations. *Photogrammetric Engineering & Remote Sensing*, Vol. 71, No. 11, pp. 1284–1294.

Carlson, G.E., and Ebel, W.J. 1995. Co-occurrence matrices for small region texture measurement and comparison. *International Journal of Remote Sensing*, Vol. 16, No. 8, pp. 1417–1423.

Chubey, M.S., Franklin, S.E., and Wulder, M.A. 2006. Object-based analysis of IKONOS-2 imagery for extraction of forest inventory parameters. *Photogrammetric Engineering & Remote Sensing*, Vol. 72, No. 4, pp. 383–394.

Coburn, C.A., and Roberts, A.C.B. 2004. A multiscale texture analysis procedure for improved forest stand classification. *International Journal of Remote Sensing*, Vol. 25, No. 20, pp. 4287–4308.

Desroches, P.R., and Yee, S.Y.K. 1999. Wavelet applications for mesocylone identification in Doppler radar observations. *Journal of Applied Meteorology*, Vol. 38, pp. 965–980.

Diggle, P.J. 2003. *Statistical analysis of spatial point patterns*. 2nd ed. Oxford University Press, New York. pp. 1–159.

Falkowski, M.J., Smith, A.M.S., Hudak, A.T., Gessler, P.E., Vierling, L.A., and Crookston, N.L. 2006. Automated estimation of individual conifer tree height and crown diameter via two-dimensional spatial wavelet analysis of Lidar data. *Canadian Journal of Remote Sensing*, Vol. 32, No. 2, pp. 153–161.

Falkowski, M.J., Smith, A.M.S., Gessler, P.E., Hudak, A.T., Vierling, L.A., and Evans, J.S. 2008. The influence of conifer forest canopy cover on the accuracy of two individual tree measurement algorithms using lidar data. *Canadian Journal of Remote Sensing*, Vol. 34, Suppl. 2. In this issue.

Gao, Y., Mas, J.-F., Matthuis, B.H.P., Zhang, X., and Van Dijk, P.M. 2006. Comparison of pixel-based and object-orientated image classification approaches — a case study in a coal fire area, Wuda, Inner Mongolia, China. *International Journal of Remote Sensing*, Vol. 27, No. 18, pp. 4039–4055.

Garrity, S.R., Vierling, L.A., Smith, A.M.S., Hann, D.B., and Falkowski, M.J. 2008. Automatic detection of shrub location, crown area, and cover using spatial wavelet analysis and aerial photography. *Canadian Journal of Remote Sensing*, Vol. 34, Suppl. 2. In this issue.

Getis, A., and Ord, J.K. 1992. The analysis of spatial association by use of distance statistics. *Geographical Analysis*, Vol. 24, pp. 189–206.

Getis, A., and Ord, J.K. 1996. Local spatial statistics: an overview. In *Spatial analysis: modelling in a GIS environment*. Edited by P. Longley and M. Batty. Geoinformation International, Cambridge, UK. pp. 261–277.

Gholz, H.L., Grier, C.C., Campbell, A.G., and Brown, A.T. 1979. *Equations for estimating biomass and leaf area of plants in the Pacific Northwest*. Oregon State University Forest Research Laboratory Research Paper 41. 39 pp.

Gougeon, F.A. 1995. Comparison of possible multispectral classification schemes for tree crowns individually delineated on high spatial resolution MEIS images. *Canadian Journal of Remote Sensing*, Vol. 21, No. 1, pp. 1–9.

Groome, G., Mucher, C.A., Ihse, M., and Wrbka, T. 2006. Remote sensing in landscape ecology: experiences and perspectives in a European context. *Landscape Ecology*, Vol. 21, pp. 391–408.

Hall, O., Hay, G.J., Bouchard, A., and Marceau, D.J. 2003. Detecting dominant landscape objects through multiple scales: An integration of object-specific methods and watershed segmentation. *Landscape Ecology*, Vol. 19, pp. 59–76.

Hann, D.B., Smith, A.M.S., and Powell, A.K. 2003. Classification of off-diagonal points in a co-occurrence matrix. *International Journal of Remote Sensing*, Vol. 24, pp. 1949–1956.

Haralick, R.M., Shanmugam, K., and Dinstein, I. 1974. Textural features for image classification. *IEEE Transactions on Geoscience and Remote Sensing*, Vol. SMC-3, No. 6, pp. 610–621.

Hudak, A.T., and Wessman, C.A. 1998. Textural analysis of historical aerial photography to characterize woody plant encroachment in South African savanna. *Remote Sensing of Environment*, Vol. 66, pp. 317–330.

Hudak, A.T., Crookston, N.L., Evans, J.S., Falkowski, M.J., Smith, A.M.S., Gessler, P.E., and Morgan, P. 2006. Regression modeling and mapping of coniferous forest basal area and tree density from discrete-return lidar and multispectral data. *Canadian Journal of Remote Sensing*, Vol. 32, No. 2, pp. 126–138.

Ishida, T., Itagaki, S., Sasaki, Y., and Ando, H. 2004. Application of wavelet transform for extracting edges of paddy fields from remotely sensed images. *International Journal of Remote Sensing*, Vol. 25, No. 2, pp. 347–357.

Johnson, D.D., and Miller, R.F. 2005. Structure and development of expanding western juniper woodlands as influenced by two topographic variables. *Forest Ecology and Management*, Vol. 229, pp. 7–15.

Jordon, G., and Schott, B. 2005. Application of wavelet analysis to the study of spatial pattern of morphotectonic lineaments in digital terrain models: a case study. *Remote Sensing of Environment*, Vol. 94, pp. 31–38.

Karathanassi, V., Iossifidis, C.H., and Rokos, D. 2000. A texture-based classification method for classifying built areas according to their density. *International Journal of Remote Sensing*, Vol. 21, No. 9, pp. 1807–1823.

Keima, J.B.K. 2002. Texture analysis and data fusion in the extraction of topographic objects from satellite imagery. *International Journal of Remote Sensing*, Vol. 23, No. 4, pp. 767–776.

Laffan, S.W. 2002. Using process models to improve spatial analysis. *International Journal of Geographical Information Science*, Vol. 16, No. 3, pp. 245–257.

Laine, A.F., Schuler, S., Fan, J., and Huda, W. 1994. Mammographic feature enhancement by multiscale analysis. *IEEE Transactions on Medical Imaging*, Vol. 13, No. 4, pp. 725–740.

Lark, R.M. 1996. Geostatistical description of texture on an aerial photograph for discriminating classes of land cover. *International Journal of Remote Sensing*, Vol. 17, pp. 2115–2133.

Leckie, D., Gougeon, F., Hill, D., Quinn, R., Armstrong, L., and Shreenan, R. 2003a. Combined high-density Lidar and multispectral imagery for individual tree crown analysis. *Canadian Journal of Remote Sensing*, Vol. 29, No. 5, pp. 633–649.

Leckie, D., Gougeon, F., Walsworth, N., and Paradine, D. 2003b. Stand delineation and composition estimation using semi-automated individual tree crown analysis. *Remote Sensing of Environment*, Vol. 85, pp. 355–369.

Leckie, D., Gougeon, F., Tinis, S., Nelson, T., Burnett, C., and Paradine, D. 2005. Automated tree recognition in old growth conifer stands with high resolution digital imagery. *Remote Sensing of Environment*, Vol. 94, pp. 311–326.

Lee, G., and Rogerson, P. 2007. Monitoring global spatial statistics. *Stochastic Environmental Research and Risk Assessment*, Vol. 21, pp. 545–553.

Lindsay, R.W., Percival, D.B., and Rothrock, D.A. 1996. The discrete wavelet transform and the scale analysis of the surface properties of sea ice. *IEEE Transactions on Geoscience and Remote Sensing*, Vol. 34, pp. 771–787.

Lucieer, A., Stein, A., and Fisher, P. 2005. Multivariate texture-based segmentation of remotely sensed imagery for extraction of objects and their uncertainty. *International Journal of Remote Sensing*, Vol. 26, No. 14, pp. 2917–2936.

MATLAB, The MathWorks, Inc. 2004. *Matlab and Simulink, version 7.0.0.27 (R14)*. The MathWorks, Inc., Natick, Mass. Available from www.mathworks.com/products/matlab/.

Miller, R.F., and Rose, J.A. 1995. Historic expansion of *Juniperus occidentalis* in southeastern Oregon. *Great Basin Naturalist*, Vol. 55, pp. 37–45.

Miller, R.F., Bates, J.D., Svejcar, T.J., Pierson, F.B., and Eddleman, L.E. 2005. *Biology, ecology and management of western juniper.* Oregon State University Agricultural Experiment Station, Technical Bulletin 152.

Palenichke, R.M., and Zaremba, M.B. 2007. Multiscale isotropic matched filtering for individual tree detection in LIDAR images. *IEEE Transactions on Geoscience and Remote Sensing*, Vol. 45, No. 12, pp. 3944–3956.

Paplinski, A.P., and Boyce, J.F. 1997. Segmentation of a class of ophthalmological images using a directional variance operator and co-occurrence arrays. *Optical Engineering*, Vol. 36, pp. 3140–3147.

Piwowar, J.M. 2008. The derivation of an Arctic Sea ice normal through temporal mixture analysis of satellite imagery. *International Journal of Applied Earth Observation and Geoinformation*, Vol. 10, pp. 92–108.

Piwowar, J.M., Peddle, D.R., and LeDrew, E.F. 1998. Temporal mixture analysis of Arctic Sea ice imagery: a new approach for monitoring environmental change. *Remote Sensing of Environment*, Vol. 63, No. 3, pp. 195–207.

Popescu, S.C., and Wynne, R.H. 2004. Seeing the trees in the forest: using lidar and multispectral data fusion with local filtering and variable window size for estimating tree height. *Photogrammetric Engineering & Remote Sensing*, Vol. 70, pp. 589–604.

Popescu, S.C., Wynne, R.H., and Nelson, R.F. 2003. Measuring individual tree crown diameter with lidar and assessing its influence on estimating forest volume and biomass. *Canadian Journal of Remote Sensing*, Vol. 29, No. 5, pp. 564–577.

R Development Core Team. 2007. *R: a language and environment for statistical computing*. R Foundation for Statistical Computing, Vienna, Austria. ISBN 3-900051-07-0. Available from www.R-project.org.

Robinson, A.P., and Froese, R.E. 2004. Model validation using equivalence tests. *Ecological Modeling*, Vol. 176, pp. 349–358.

Robinson, A.P., Duursma, R.A., and Marshall, J.D. 2005. A regression-based equivalence test for model validation: shifting the burden of proof. *Tree Physiology*, Vol. 25, pp. 903–913.

Strand, E.K., Smith, A.M.S., Bunting, S.C., Vierling, L.A., Hann, D.B., and Gessler, P.E. 2006a. Wavelet estimation of plant spatial patterns in multi-temporal aerial photography. *International Journal of Remote Sensing*, Vol. 27, No. 9–10, pp. 2049–2054.

Strand, E.K., Robinson, A.P., and Bunting, S.C. 2006b. Spatial patterns on the sagebrush-steppe/Western juniper ecotone. *Plant Ecology*, Vol. 190, pp. 159–173.

Strand, E.K., Vierling, L.A., Smith, A.M.S., and Bunting, S.C. 2008. Net changes in aboveground woody carbon stock in western juniper woodlands, 1946–1998. *Journal of Geophysical Research, Biogeosciences*, Vol. 113, G01013. doi:10.1029/2007JG000544.

Tenorio, L., Jaffe, A.H., Hanany, S., and Lineweaver, C.H. 1999. Applications of wavelets to the analysis of cosmic microwave background maps. *Monthly Notices of the Royal Astronomical Society*, Vol. 310, pp. 823–834.

Ter-Mikaelian, M.T., and Korsukhin, M.D. 1997. Biomass equations for sixty-five North American tree species. *Forest Ecology and Management*, Vol. 97, pp. 1–24.

Turner, M.G., Gardner, R.H., and O'Neill, R.V. 2001. *Landscape ecology in theory and practice*. Springer-Verlag, New York. 401 pp.

USDA-NRCS. 1998. *Owyhee County digital soil survey*. Natural Resources Conservation Service, US Department of Agriculture (USDA-NRCS), Washington, D.C.

Vu, T.T., Tokunaga, M., and Yamazaki, F. 2003. Wavelet-based extraction of building features from airborne laser scanner data. *Canadian Journal of Remote Sensing*, Vol. 29, No. 6, pp. 783–791.

Wang, L., Gong, P., and Biging, G.S. 2004a. Individual tree-crown delineation and treetop detection in high-spatial-resolution aerial imagery. *Photogrammetric Engineering & Remote Sensing*, Vol. 70, No. 3, pp. 351–357.

Wang, L., Souza, W.P., and Gong, P. 2004b. Integration of object-based and pixel-based classification for mapping mangroves with IKONOS imagery. *International Journal of Remote Sensing*, Vol. 25, No. 24, pp. 5655–5668.

West, N.E. 1999. Juniper–pinyon savannas and woodlands of western North America. In *savannas, barrens, and rock outcrop plant communities of North America*. Edited by R.C. Anderson, J.S. Fralish, and J.M. Baskin. Cambridge University Press, London, UK. pp. 288–308.

Wu, S.Y., and Liu, A.K. 2003. Towards an automated ocean feature detection, extraction and classification scheme for SAR imagery. *International Journal of Remote Sensing*, Vol. 24, No. 5, pp. 935–951.

Wulder, M.A., White, J.C., Niemann, K.O., and Nelson, T. 2004. Comparison of airborne and satellite high spatial resolution data for the identification of individual trees with local maxima filtering. *International Journal of Remote Sensing*, Vol. 25, pp. 2225–2232.

Young, J.A., and Evans, R.A. 1981. Demography and fire history of a western juniper stand. *Journal of Range Management*, Vol. 34, pp. 501–506.

Zhan, Q., Molenaar, M., Tempfli, K., and Shi, W. 2005. Quality assessment for geo-spatial objects derived from remotely sensed data. *International Journal of Remote Sensing*, Vol. 26, No. 14, pp. 2953–2974.

Zhang, Y.J. 1996. A survey on evaluation methods for image segmentation. *Pattern Recognition*, Vol. 29, No. 8, pp. 1335–1346.

Zhang, Y.J. 1997. Evaluation and comparison of different segmentation algorithms.
Pattern Recognition Letters, Vol. 18, No. 10, pp. 963–974.

Zhang, Y.J., and Gerbrands, J.J. 1994. Objective and quantitative segmentation evaluation and comparison. *Signal Processing*, Vol. 39, No. 1–2, pp. 43–54.

Zhang, X., Younan, N.H., and O'Hara, C.G. 2005. Wavelet domain statistical hyperspectral soil texture classification. *IEEE Transactions on Geoscience and Remote Sensing*, Vol. 43, No. 3, pp. 615–618.

Zhang, H., Fritts, J.E., and Goldman, S.A. 2008. Image segmentation evaluation: a survey of unsupervised methods. *Computer Vision and Image Understanding*, Vol. 110, No. 2, pp. 260–280.

Smith A.M.S., Wooster M.J., Powell, A.K. and Usher, D., 2002, Texture based feature extraction: application to burn scar detection in Earth Observation Imagery, International Journal of Remote Sensing, Vol. 23, pp. 1733-1739.

Definies, 2007. Definies Developer 7, Reference Book, Definies AG, Munich, Germany, 195 pp.